7

Nanophysical approach to diagnosis of epithelial tissues using Opto-magnetic imaging spectroscopy

Lidija Matija, Branislava Jeftić, Gorana Nikolić, Aleksandra Dragičević, Ivana Mileusnić, Jelena Munćan, Djuro Koruga

Nanolab, Deparment of Biomedical Engineering, Faculty of Mechanical Engineering, University of Belgrade, Belgrade, Serbia.

Outline:

Introduction

Cancer is a broad group of diseases involving unregulated cell growth. Inside the tissue where the cancer occurs (a malignant neoplasm) cells divide and grow uncontrollably and form malignant tumours, which invade nearby parts of the body. Cancer also spreads to distant parts of the body through the lymphatic and blood circulatory system [1]. The incidence and mortality of tumours are on the increase from year to year. For example, cervical cancer is the seventh most common cancer in both sexes and the third most common cancer among women, which is caused by high-risk HPV infections. HPV types 16 and 18 are responsible for 70% of all cervical cancers. High-risk HPV also causes anal, vaginal, vulvar, penile cancer and cancer of the oropharynx [4]. In 2008 an estimated 530,000 women across the world were diagnosed with cervical cancer, which accounted for nearly one in ten (9%) of all cancers diagnosed in women and resulted in 275,000 deaths, around 8% of all female cancer deaths. Colorectal (including anal) cancer is the third most common cancer and the fourth cause of cancer deaths worldwide. Statistic data for 2008 showed that 1.24 million people had been diagnosed with colorectal cancer, accounting for 10% of all cancers and responsible for almost 610,000 deaths [2]. Skin cancer is the most common cancer in Australia, New Zealand and the United States. More than 3.5 million skin cancers (non-melanoma cancer) in over two million people are diagnosed annually in the USA [3]. Melanoma accounts for less than five per cent of skin cancer cases and the majority of skin cancer deaths [4]. In the UK, in 2011, there were 2,209 deaths from malignant melanoma skin cancer, in 2010 around 100,000 people were diagnosed with non-melanoma skin cancer and in 2011 there were 585 deaths from non-melanoma skin cancer [5].
A new approach to the detection of abnormalities in epithelial tissue will be presented in this chapter. Several types of epithelial tissue such as skin, cervix and colon were investigated in these studies due to their increasing incidence and mortality rate which is still unacceptably high, even though the existing diagnostic tests have greatly improved in recent years. Various techniques are in use for the detection of cancer of epithelial tissue (Pap test, HPV testing, colposcopy, curettage, histopathology, cytology, colonoscopy as a “gold standard’’, etc.), but some of them are very expensive, some of them cannot be used for some patients because of contra-indications (for example, patients with stent cannot use NMR as a diagnostic method), etc. We designed and made a prototype optical device for non-invasive use, which does not cause (to our knowledge) any contra-indications.

Epithelial tissue

Epithelium, along with connective tissue, muscle, and nerve, is one of the four primary tissue types in the human body. It is commonly found as a covering or lining for other types of hollow organs, as in the case of the epidermis and the lining of the entire gastrointestinal tract, and constitutes most of the glandular tissue. Epithelial tissues are avascular (no blood vessels), composed of layers of tightly packed cells connected by intercellular nexus and with a minimal content of extracellular matrix and interstitial fluid. The amount of extracellular matrix and interstitial fluid is extremely small and therefore invisible under a light microscope. Beneath the epithelial cells lies a very thin glycoprotein layer of extracellular matrix, the basement membrane, which serves to anchor the epithelium to the connective tissue below and is made up of two distinct layers called basal and reticular lamina. Basal lamina is very thin, and also invisible under a light microscope, while the basement membrane is just barely visible in specially-stained sections. This membrane contains collagen, adhesive glycoproteins

called laminin and fibronectin, and a large protein-carbohydrate complex called heparan sulphate, which gradually blends with collagenous and reticular fibres on the connective tissue side.

Histological differences among the various epithelia are based on the shapes of the cells, the number of cell layers present, various modifications to the surfaces of the cells that can be seen under a light microscope (microvilli, stereocilia, cilia), and characteristic patterns of reaction with particular dyes (acidophilia, basophilia, special stains). Epithelial tissues have numerous particular functions; in general, their functions are to mediate absorption, excretion, protection, secretion, sensory reception and transport.

Epithelial tissues are divided into 1) *simple*, which is with one layer and one type of cells (squamous, cuboidal, columnar), 2) *stratified*, two and more layers and one or more types of cells and 3) *pseudostratified*, one layer that appears to be more than one layer. In this chapter, several types of epithelial tissues will be presented, with their optical and biophysical characteristics, which are parts of organs such as the skin, the large intestine, and the cervix of the uterus [6-10].

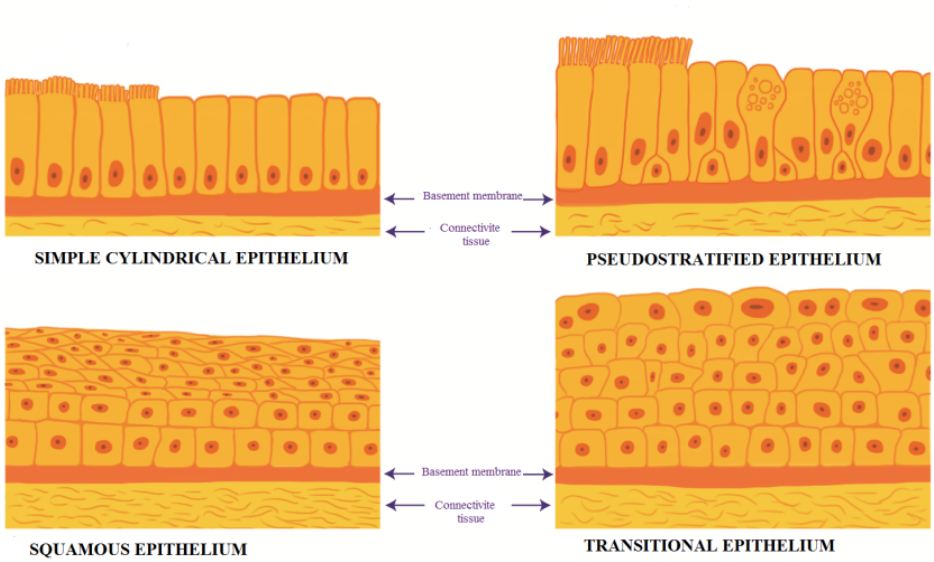

FIGURE 7.1
Examples of main types of epithelial tissue

The skin: covers the entire outer surface of the human body, except for one part of the eye and the area of natural openings (nasal, oral, anal and genital), and becomes appropriate mucosa. It is the largest organ and weighs from 5 to 17 lbs (16% of the total body weight) and with a total area of 10 to 25 ft^2. It consists of three main parts: the epithelial tissue – the upper layer of the skin, the dermis - the middle layer, and the fat connective tissue (hypodermis) - the deepest layer of the skin, which connects with the muscles and bones. The epidermis is keratinized stratified squamous epithelium and is the surface layer of the skin. It is made of keratinocytes (95%), melanocytes, Langerhans cells and Merkel cells. Keratinocytes are the main and most numerous cells that produce keratin and also synthesize: specific proteins (that form the inner lining of keratinized cells), products such as cytokines, enzymes, proteins, inflammatory mediators (that are important when it comes to the inflammatory process). Melanocytes are the cells that synthesize pigment melanin, which protect the skin from the harmful

effects of UV rays. The number of melanocytes is constant per unit volume, and one melanocyte serves 4-10 keratinocytes.

The layers of epidermis are: *stratum basale, stratum spinosum, stratum granulosum, stratum lucidum (only in the epidermis on the palm and the sole of the foot) and stratum corneum.* Stratum basale or the basal layer is the deepest layer of epidermis, consisting of one line (row) of cylindrical cells. Ultrastructural analysis shows that the basal cells transform into keratinocytes, which means that the basal cell is a stem cell from which multiplication begins. Stratum spinosum or the spinous layer has several layers of large polygonal cells which are tightly interconnected with the nexus, called desmosomes. In this layer the transformation of the keratinocytes continues. Stratum granulosum or granulosa layer consists of several flat, polygonal cells. In this layer, the transformation of a keratinocyte continues. Stratum corneum or the horny corneal layer consists of 15-20 layers of flat, dead cell, called corneocytes. In this layer the keratinization process is completed. Corneocytes separate from each other and gradually the whole process ends with desquamation (peeling), and the cells of basal layer renew the epithelium. It takes about 30 days to restore the stratum corneum. This means that during this time the cells of the basal layer divide, multiply, and go through all the layers of skin to become corneocytes in the stratum corneum. The dermis or the loose connective tissue is just under the epidermis. Components of the dermis provide mechanical support, rigidity and thickness (1–4 mm). The dermis is composed of two layers: papillary and reticular. Loose connective tissue and extracellular matrix consist of collagen fibres (collagen type I and III) and elastin, which form the basis of the papillary layer of the dermis. Irregular loose thick connective tissue is the basis of the reticular layer. The dense network of the thick erratically positioned collagen bundles, which lies parallel to the surface of the skin in the direction of the force stretching the skin, provides mechanical stability. The hypodermis is the deepest layer of the skin, composed of lobules of adipose tissue separated by connective tissue. It is a thermal insulator, the depot of energetic materials and binds the skin to the muscle and bones, providing its mobility. The boundary between the dermis and the epidermis is the basement membrane, which is important because of its prognostic significance of skin tumours. If it is intact, then it is an indication that the disease is in the early stages, located only in the epidermis and that a cure is almost 100%. However, if it is compromised, the outcome depends on which tissue is affected, the biological potential of the tumor spreading to other parts of the body, i.e. secondary deposits. [9, 11-17].

The Cervix: The womb (*uterus*) is the internal female sex organ. It is located in the pelvic region called the *cavum pelvis.* The uterus has four major parts: a curved upper area in which the fallopian tubes connect to the uterus (*fundus uteri*), the body (*corpus uteri*), the narrow neck region (*isthmus uteri*), and the lowest section is the cervix (*cervix uteri*), which ends in the cavity of the vagina and is the connection between the uterus and vagina. The uterus is 2.4 to 3.1 inches long; its wall is approximately 0.8 to 1.2 inches thick. The width of the organ varies; it is 2.4 inches wide at the fundus and half at the isthmus. The uterus is located between the bladder (front) and the large intestine (back). The cervix is the narrowed lowest part of the uterus. It has the shape of a cylinder and consists of two parts: an upper (*portio supravaginalis*) and lower (*portio vaginalis*) part. Inside the cervix is a canal (*canalis cervicis*) which leads into the uterus.

Histologically, the uterus is composed of three layers: perimetrium myometrium and endometrium. The perimetrium is a serous membrane which envelops the uterus. The myometrium consists of three layers of muscle tissue (longitudinally, circularly and obliquely). Between these layers is a connective tissue, blood vessels, collagen and elastin fibres. The endometrium lines the cavity and changes its width during the menstrual cycle and during ovulation. The cervix is covered with two types of cells: squamous cells which are the outer part, called the *exocervix* (the part which is connected to the

vagina) and glandular cells which are present in the cervical canal (endocervix). The squamous epithelium is composed of 15 to 20 rows of cells and does not possess blood vessels or connective fibres, therefore the nutrients are transferred through the capillary system by diffusion. The glandular epithelium is composed of one row of cells which produce mucus. These two types of epithelia converge at a place called the *transformation zone.* This zone proliferates under the influence of sex hormones, particularly estrogen when the menstrual cycle begins. The transformation zone moves during the lifetime and does not always match with the external orifice of the cervix and is the place where all precancerous and cancerous lesions begin [18, 19].

The Colon: The digestive system includes the alimentary canal and its principle associated organs such as tongue, teeth, salivary glands, pancreas, liver and gallbladder and the anatomical parts are: the oral cavity, the esophagus and the gastrointestinal tract (the stomach, the small intestine and the large intestine) [20]. The main functions of the digestive system are chewing and swallowing food and saliva, absorption of nutrient material and the elimination of undigested food and waste. Our region of interest is the large intestine, especially the colon and the rectum. The colon, which is the biggest part of the gastrointestinal tract, histologically consists of four layers: the inner layer - the mucosa, the connective tissue - the submucosa, the muscle tissue – the muscularis externa and the outer layer - the adventitia or serosa. The epithelium of the colon is the simple columnar, made up of several different types of cells. The main functions of these cells are: absorption, protection and secretion. Numerous tubular glands extend through the full thickness of the mucosa and they consist of the same epithelium as the colon. Stem cells are in the deepest part of the intestinal gland and because of their capability to proliferate and differentiate, the epithelial cells can renew themselves. The cells of the mucosal epithelium are: the columnar absorptive cells (whose role is the reabsorption of electrolytes and water), goblet cells (which continuously secrete mucus), caveolated “tuft” cells - a form of exhausted goblet cells and, enteroendocrine cells (which produce various paracrine and endocrine hormones). The connective tissue or submucosa contains a thick layer of collagen and proteoglycans, pericryptal fibroblast sheaths, immune defence cells, nerve plexus, lymphatic and blood vessels. This layer of collagen and proteoglycans regulate water and transport electrolytes from the intercellular compartment to the vascular compartment. The muscularis externa contains two concentric layers of smooth muscle (cells of both layers form a tight spiral): the inner layer is a circularly oriented layer, and the outer layer is a longitudinally oriented layer. The muscularis externa produces contractions. Two different types of contractions exist: segmentation (does not result in the propulsion of contents) and peristalsis (results in the distal mass movement of colonic contents). The outer layer, called adventitia, exists when the large intestine is in direct contact with the other structure, otherwise the outer layer is called serosa. Serosa consists of a layer of simple squamous epithelium and connective tissue, with large blood vessels, lymphatic vessels and nerve trunks [20, 21].

Optical methods

Conventional screening methods used in clinical practice are time limiting and expensive. As such, these medical techniques are available only to a certain section of the world's population. Screening and early detection of cancer could significantly improve the optical methods which are present in modern scientific research. Some of them even allow visualization of the tissue structure at subcellular level, thus providing the necessary information for identification of precancerous lesions.

Optical spectroscopic methods such as Raman spectroscopy, FTIR (Fourier Transform Infrared) and fluorescence spectroscopy proved to be a good alternative method for the detection of neoplastic changes in cervical tissue [22-24], different types of colon cancer [23, 25, 26] and skin cancer [23, 25, 27]. These methods are fast, objective, and can be developed for *in vivo* screening of diseases, which would exclude the need for painful biopsies. The main advantage of these methods is the possibility of providing information about the biochemical, structural and pathophysiological changes which occur in the tissue, but these methods are not routinely used in clinical practice, since they are still only research tools.

FTIR (Fourier Transform Infrared) spectroscopy is a method which has only recently been applied in the detection of various types of cancer, and as such is being tested in research of the screening of cervical cancer [22]. FTIR detects irregularities in the cells on a molecular level. This distortion preceded the development of morphological changes that are available to detect under a microscope, showing the great importance of FTIR spectroscopy for early detection of precancerous lesions. In the case of colon cancer detection, FTIR showed good results, especially during an operation. Experimental results revealed that the spectral characteristics of normal and malignant tissues found *in vivo* and *in situ* were similar to those obtained from *in vitro* measurements in our previous fundamental research [23]. For this kind of cancer, it is very difficult to apply any spectroscopy *in vivo*, which is why it is important to compare the results between *in vivo* and *in vitro* spectroscopy.

The advantages of Raman spectroscopy over the other optical methods include high spatial resolution (up to 1 μm), the use of less harmful NIR radiation, less demanding preparation of the samples and its application to *in vivo / in situ* measurements. Over the years, various algorithms have been developed for the differentiation of tissue in order to examine the feasibility of using Raman spectroscopy for the detection of cervical precancerous conditions. Some investigations used empirically selected peak intensities and the intensity of these relationships to distinguish precancerous conditions from other tissues. Other algorithms for differentiating diseased from healthy tissue used statistical methods based on PCA (Principal Component Analysis) [24]. Near-infrared Fourier Transform Raman spectroscopy is an analytical, non-destructive technique that provides information about the molecular structure of the investigated sample. The molecular structure of proteins and lipids differ between neoplastic and normal tissues and therefore Raman spectroscopy has been considered promising for the diagnosis of cancer. In the Raman spectra, the secondary structure of the proteins was reflected by the amide vibrations of peptide bonds. It is the most frequently used spectroscopy for the detection of skin lesions [25]. Raman spectroscopy is also suitable for the diagnosis of colon carcinoma because of the sensitivity of the method in detecting small molecular changes that are characteristic for cancer, such as the ratio between an increased nucleus and cytoplasm, disorganized chromatin, increased metabolic activity and changes in the level of fats and proteins [26].

Infrared spectroscopy is widely perceived as a future clinical technology for cancer detection and grading for all types of epithelial lesions. For example, melanoma could be differentiated from the epidermis using parameters derived from absorbance bands originating from molecular vibrations of nucleic acids and/or their bases. Additionally, absorbance from tyrosine and phosphate that are abnormally elevated in malignant melanoma could be used as markers [27].

Despite all the benefits of the stated spectroscopy which these methods could bring to future clinical trials, there are still some issues concerning the implementation of these methods in clinical practice.

Method

In order to meet the objectives for a more successful method for early detection of epithelial tissue cancer, with a lower cost price, we have developed an Opto-magnetic image spectroscopy (OMIS). The OMIS was first introduced as a non-invasive method for skin characterization, in 2009 [28]. Since then, it has evolved and has been adjusted for a wider area of applications in biomedical engineering; polymers, liquids and epithelial tissues (healthy and cancer) [29-32].
The method obtains paramagnetic/diamagnetic properties of materials (unpaired/paired electrons) based on their interaction with visible light. The basic tool is the light of wavelength in a range between 400 nm and 700 nm provided by white light emitting diodes (LED, Nichia, 150 mA, 3V, maximum relative emission intensity at 450 nm wavelength, chromaticity x=34.4 and y=35.4, ambient temperature 25^{o}C). Since energy of valence electrons and photons of visible light has the same value, imaging by visible light is non-invasive and provides an examination process that can be repeatedly conducted without presenting any risks to the patient or sample material damage. Finally, due to the numerous advantages that the digital image acquisition offers, the design of this technique and customized hardware solution used in the studies have been further developed. The OMIS technique has yielded positive results in early detection of cancer of epithelial tissues such as the cervix, the colon, the skin and other biological samples, which are presented in this chapter. The method is applicable both *in vitro* and *in vivo*.

Physical background

Opto-Magnetic Imaging Spectroscopy (OMIS) is a nanophysical diagnostic technique based on the interaction of electromagnetic radiation with valence electrons within the sample material, and therefore examines the electronic properties of the matter (covalent bonds, hydrogen bonds, ion-electron interaction, and Van der Waals interaction). Bearing in mind that the orbital velocity of a valence electron in atoms is approximately 10^{6} m/s, the calculated ratio is $F_M/F_E \approx 10^{-4}$ between the magnetic force (F_M) and the electrical force (F_E) of matter. Since force (F) is directly related to action (A= F x d x t, where F is the force in the range 0.01 – 1.0 nN, d is the displacement in the range 0,1 – 5.0 nm, and *t* is time in the range 10^{-8}-10^{-10}s) [31,33], it can be concluded that the magnetic force of matter is four orders of magnitude closer to the quantum state of matter than the electrical force. This opens an opportunity to detect the conformational states and changes in the matter on a nanoscale level using a light-matter interaction method.

The fact that the magnetic force of valence electrons is more closely related to the quantum states of matter, it primarily influences the choice of magnetic interaction as a main measurement modality. The optical modality was chosen because the photons of visible light are perfect probes for states of valence electrons of matter with respect to their sufficiently low energy levels and sensitivity.

The light as an electromagnetic phenomenon consists of electric and magnetic waves that are perpendicular and can be split under specific conditions, which means that the light can be polarized. One particular type of polarization of light occurs during the interaction of light and matter at a specific angle, known as Brewster's angle. Each type of matter has a unique angle value of Brewster's angle, for example, Brewster's angle for water-air interface is 53° (refractive index n=1.33) [34]. When a sample is illuminated under this specific angle, the reflected light will be polarized. Reflected polarized light contains only an electrical component in a longitudinal wave, and a magnetic component in a transversal wave (perpendicular to longitudinal) of light-matter interaction. Since the longitudinal wave directly influences CCD/CMOS sensor, while the transversal has a neglected influence, then by

subtracting the reflected polarized light (electrical properties) from the reflected white diffuse light (electromagnetic properties), the result will provide information about the magnetic properties of matter based on light-matter interaction.

If a digital image of a material surface is acquired using classical optical microscope equipped with a digital camera, it represents the reflectance of the sample and thus contains information about it. If the sample is illuminated with the white diffuse light, the reflected light waves will have an electromagnetic nature. However, if the sample is illuminated with white light under Brewster's angle, specific for that type of sample material, the reflected light will have an extremely dominant electric nature (Figure 7.2). Advancements in the field of digital image processing have made it possible to do various operations with digital images. This means that as much information as possible can be extracted from the properties of the sample. Theoretically, if a digital image of a sample is acquired using illumination under Brewster's angle, and subtracted from the image of the same sample acquired using illumination with diffuse white light, then the resultant image would represent a sort of composite image or a map of the magnetic properties of that sample.

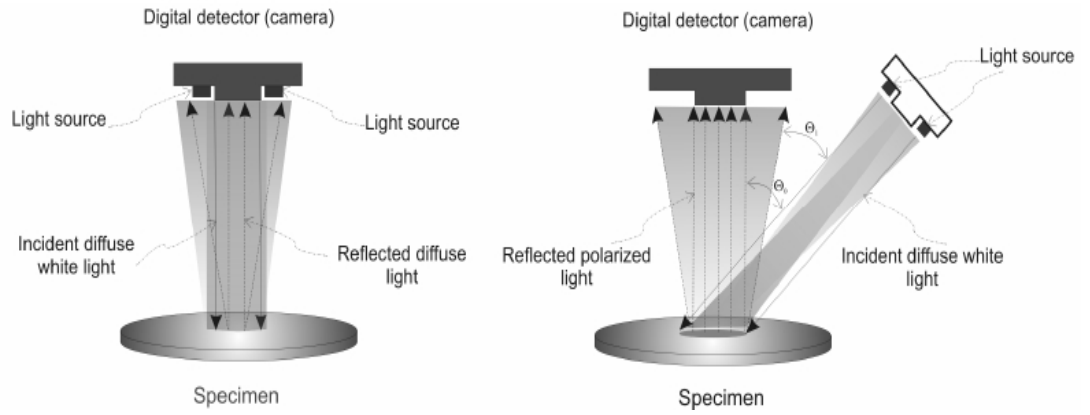

FIGURE 7.2
The experimental arrangement sketch shows the relative positions of light sources for white (a) and reflected polarized light (b). The degree of light polarization is 95.4%, while angular diffusion of the light source (six white LEDs arranged in a circle) is ±1:6° (the difference between the angles θ and θ_1) [28,30]

The digital images acquired using OMIS method are RGGB (red, double green, and blue) images because the camera is adapted for the human eye (the visual system). The algorithm for the image processing is thus based on the "Maxwell triangle" chromaticity diagram and it allows the conversion of the digital image to Opto-magnetic spectra through several operations, starting with the creation of histograms for each colour channel and subsequent conversion of the histograms to spectra [28]. A pair of digital images of the sample acquired under white diffuse light, and white diffuse light under Brewster's angle will result in three spectra, blue, red and green, for each image. When blue, green or red spectra for the image of the sample taken under Brewster's angle are subtracted from the blue, green or red spectra for the image of the sample taken under white diffuse light, the resultant composite spectrum will represent an opto-magnetic spectrum of the sample. This resultant spectrum is presented in the coordinate system, where the x axis presents the wavelength difference (WD) measured in nanometers, and the y axis as the intensity in normalized arbitrary units. The spectrum is given a designation, made from several abbreviations, which describes what kind of transformation is

performed. For example, the designation (R-B)&(W-P) means that the Opto-magnetic spectra of the imaging matter is developed by subtracting the blue colour channel spectrum (B) from the red colour channel spectrum (R); where each colour channel spectra were first developed by subtracting the colour channels spectra for image under Brewster's angle (P, as in reflected "polarized") from the image under diffuse white light (W). Similarly, various combinations can be performed. Since blue light is reflected from the surface (and a very/very thin layer) and red light from the deep tissue layers, then the most commonly (R-B)&(W-P) type of Opto-magnetic spectra is used for tissue samples. In this case we avoid the reflection from the surface (like a natural reflected mirror effect), because we need information about the tissue characteristics.

In cancer research, the application of the Opto-magnetic imaging spectroscopy method is used to discover the differences between the paramagnetic/diamagnetic state of water in healthy and cancerous tissues. Therefore, Brewster's angle of 53° for air-water interface is used whenever this method is applied in cancer research. Cancer cells contain more free water than normal cells, about 21% , [35] and the degree of malignancy increases with the degree of cell hydration [36, 37]. The disrupted state of water in cancer cells is used as a parameter for cancer detection and even for treatment [37].

The described properties of Opto-magnetic imaging spectroscopy provide a basis for an excellent environment for screening testing, where speed, ease of use, accuracy and low cost equally contribute to the successful early diagnosis of cancer. The measuring repeatability of OMIS for the same sample is: 98.8±1.2 %, 97.8±2.2% and 96.9±3.1%, for solid state matter, viscoelastic matter (tissues) and liquids, respectively.

Operational setup for Opto-Magnetic Imaging Spectroscopy

Device and software for Opto-Magnetic Imaging Spectroscopy are developed at the Faculty of Mechanical Engineering, University of Belgrade at the Department of Biomedical Engineering.

The basic operational setup for Opto-Magnetic Imaging Spectroscopy (OMIS) consists of a customized housing for a Canon digital camera (model IXUS 105, 12.1 MP) with a system of emission diodes at the appropriate angle and a sample holder (Figure 7.3). The illumination system consists of six LED diodes (Nichia, STS-DA7-3195) arranged in a circle and placed in front of the camera lens, providing illumination of the sample with white diffuse light and white diffuse light under Brewster's angle.

Due to specific sample requirements, the basic setup was further modified. Thus, there are three types of devices presented in Figures 7.4, 7.5 and 7.6. The first system was designed for acquiring digital images of cytology samples spread on microscopic slides (smears), (Figure 7.4), while the second system provides the same, but with the possibility of sample magnification using an optical microscope (Keyence magnifying system, model VH-Z100) (Figure 7.5). The third system enables the acquisition of digital images of tissues for conditions *in vivo* and in *vitro* (Figure 7.6).

FIGURE 7.3
The basic operational setup of the Opto-Magnetic Imaging Spectroscopy (OMIS) (NanoLab, Faculty of Mechanical Engineering, University of Belgrade)

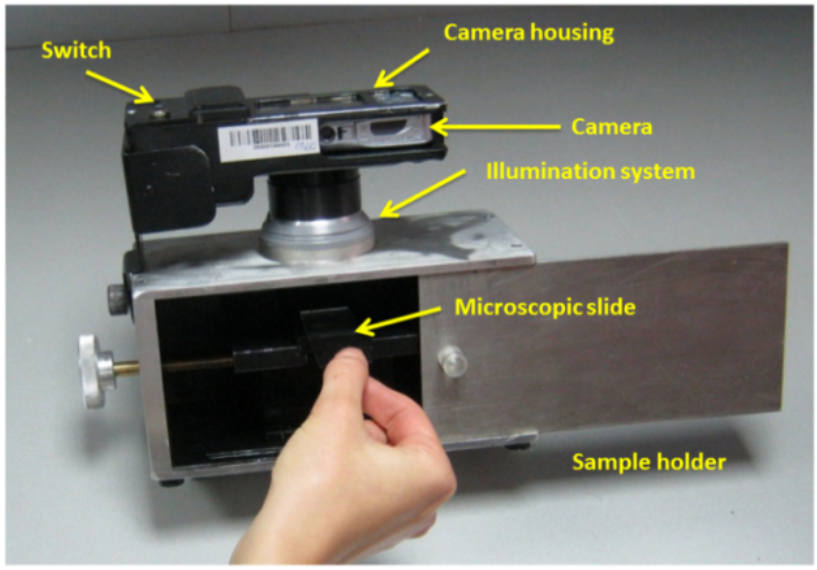

FIGURE 7.4
Opto-magnetic imaging spectroscopy system for *in vitro* applications (NanoLab, Faculty of Mechanical Engineering, University of Belgrade)

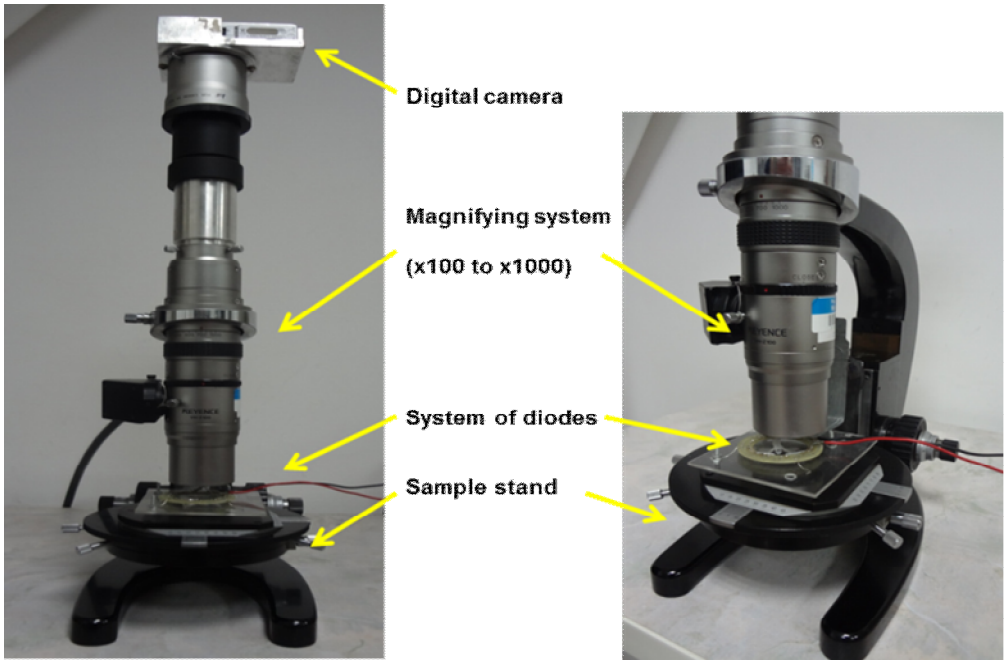

FIGURE 7.5
Opto-magnetic imaging spectroscopy system for *in vitro* applications with the possibility of sample magnification using an optical microscope (NanoLab, Faculty of Mechanical Engineering, University of Belgrade)

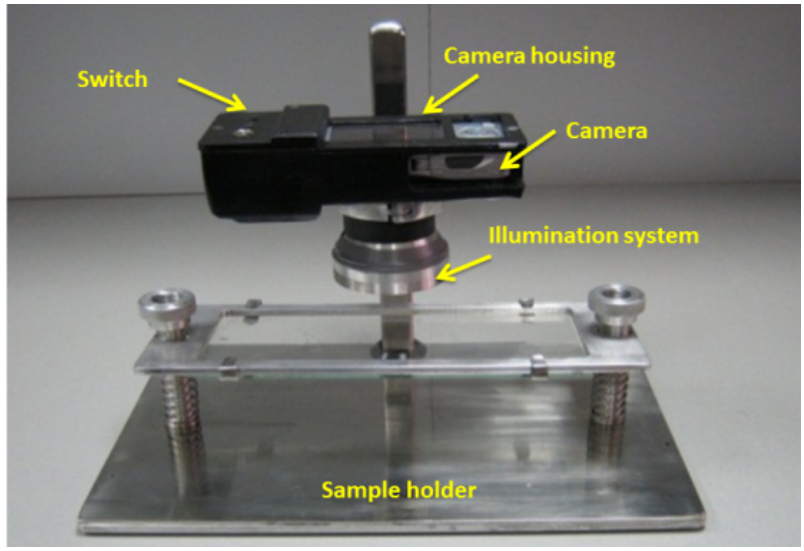

FIGURE 7.6
Opto-magnetic imaging spectroscopy system for *in vitro* applications (NanoLab, Faculty of Mechanical Engineering, University of Belgrade)

The OMIS procedure consists of:

1. Illuminating the sample with white diffuse light.

2. Acquisition of the first digital image.

3. Illuminating the sample with white diffuse light at Brewster's angle.

4. Acquisition of the second digital image.

After acquiring images, which lasts approximately 5-10s per sample for both digital images, they are processed using a code developed in the MATLAB package [28].

Material

The Cervix

Sample preparation varies depending on the method used for cancer detection and diagnosis. The main screening test for cervical cancer detection is the Papanicolaou test (Pap test or Pap smear). The cervical cells are taken with a wooden scraper and a cervical brush and are then placed on glass microscopic slides. Cells scraped from the surface of the cervix are usually placed on one microscopic slide and cells scraped from the inside of the cervical canal are placed on another slide. After adding a fixative, cells are stained and then analysed under a microscope. This conventional Papanicolaou procedure is used to detect precancerous and cancerous changes in cervical cells. The procedure includes sample staining with haematoxylin, orange and polychrome stain, and ethanol washing after each of these stains has been added to the sample. The Pap test categorizes samples into four groups: PAP group 2 (atypical cells with no evidence of malignancy), PAP group 3 (cells suspicious of malignancy), PAP group 4 (few definitive malignant cells) and PAP group 5 (large number of malignant cells). Liquid-based Cytology (LBC) is a slightly different cervical sampling method and involves obtaining cervical cells with a spatula and immersing the spatula in a liquid solution. The samples are prepared through an automated process [38]. LBC is supposed to increase sensitivity and specificity achieved with conventional Pap cytology and improves specimen quality and is widely used in developed countries. However, unsatisfactory results are still present. There is a possibility of overcoming the problems that lead to unsatisfactory results by reprocessing the samples [39], but it is a part of our current investigations.

In the studies examining different types of optical spectroscopy (FTIR, fluorescence, Raman spectroscopy), applied as diagnostic tools, spectra are usually obtained from unstained cytology (usually LBC is used) and/or tissue samples (samples cut by microtome) [22, 40, 41].

Opto-magnetic Imaging Spectroscopy uses conventionally prepared cervical samples stained according to standard Papanicolaou procedure. Slides are first screened by a cytotechnologist, and then using OMIS. Ten cervical cell OMIS spectra are averaged per each patient to obtain a single spectrum for every microscopic slide, i.e. cervical smear. The study of the stained cervical cytology samples obtained from 140 patients (280 microscopic slides with cervical cell samples), which included 35 cases from each Pap group, showed a good potential of OMIS to characterise samples from different Pap groups [42]. Authors reported problems concerning inadequate sample preparation, i.e. overstraining of the samples [43].

The Colon

The primary aim of the use of the Opto-magnetic imaging spectroscopy is to provide a non-invasive method for the differentiation between healthy and tumour tissue. *In vitro* optical properties were investigated in two kinds of tissue, healthy tissue and colonic adenocarcinoma. Tissue samples were obtained from 70 human patients with colonic adenocarcinoma, with histopathology proof. Tumours were of various grades and stages. The group included patients of both sexes, aged 19 to 85 years. After surgical resection, each removed colon sample was first rinsed with aqua purification to exclude surface blood and then placed on equipment especially designed for OMIS. Digital images of healthy tissue and neoplasms were taken ten times per each sample under white diffuse and polarized light, 1 hour and 4 hours after removal of the tissue. The imaging of healthy tissue was at least 8cm from the tumour. After imaging, the tissue sample was fixed in formalin for further histopathology examination.

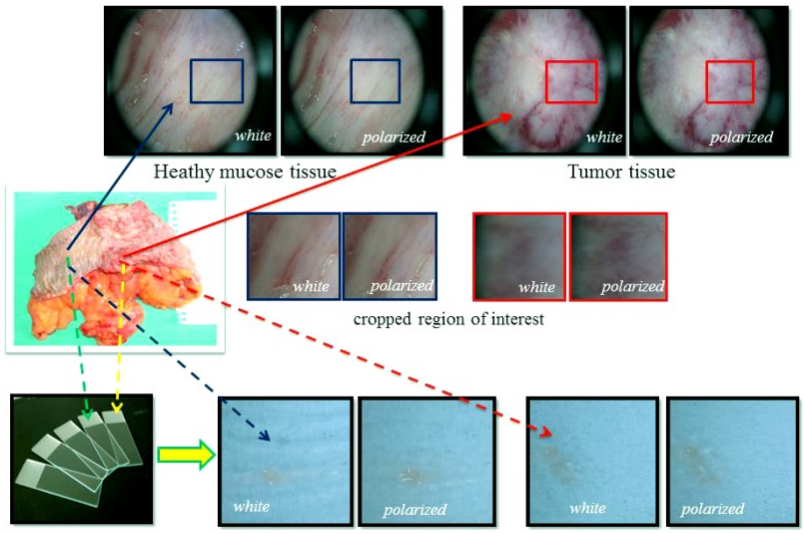

FIGURE 7.7
Colon sample and regions of interest for imaging (healthy and tumour)

Skin

Optical properties of skin *in vivo* condition were investigated for two different types of skin lesions that exist or occur on the skin due to damage. These changes were divided into two basic categories, benign and malignant pigment changes, and each category was further divided into appropriate subgroups. The device was put directly onto the lesion. Pictures were taken both with white diffuse and polarized light. In 97% of cases, the results obtained using OMIS coincided with dermoscopy and histopathology findings. Samples were obtained from 96 patients (48 samples belong to the melanoma group and the other 48 to the nevus group).

Results

The diagnosis of cervical epithelial tissue using the Opto-magnetic imaging spectroscopy

When all of the digital images of the cervical samples were obtained using the OMIS device (Figure 7.8), the data were processed using an algorithm developed to differentiate normal from cancerous cells. The differentiation is based on the OMIS spectra and considers two components from the spectra: peak intensity and the wavelength difference range where peaks appear.

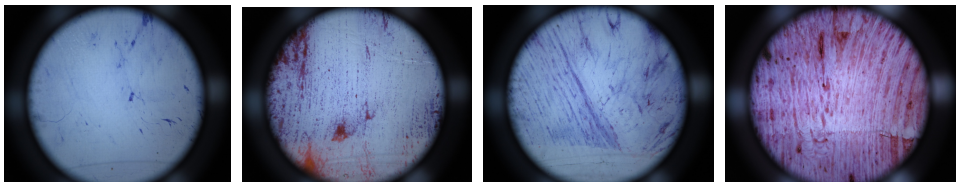

FIGURE 7.8
OMIS digital images of cervical samples belonging to II, III, IV and V Pap group (from left to right)

Figures 7.9, 7.10, 7.11 and 7.12 show the OMIS spectra of normal cervical cells (II Pap group), cells suspicious of malignancy (III Pap group), malignant cells (IV Pap group) and a large number of malignant cells (V Pap group), respectively. Spectral differences observed between these four categories reflect in intensity variations. Peak intensities of malignant cells are lower than peak intensities of normal cervical cells. There is also a noticeable shift in peak positions. Figure 7.13 shows the OMIS spectra of samples from all four Pap groups.

Peak intensity variations in the spectra of different cervical samples within each Pap group are assumed to be present due to inadequate sample preparation and over staining. In order to overcome these problems, OMIS was conducted on non-stained cervical samples. This study is still in progress and so far gives good results, but still needs a larger group of patients from all four Pap groups.

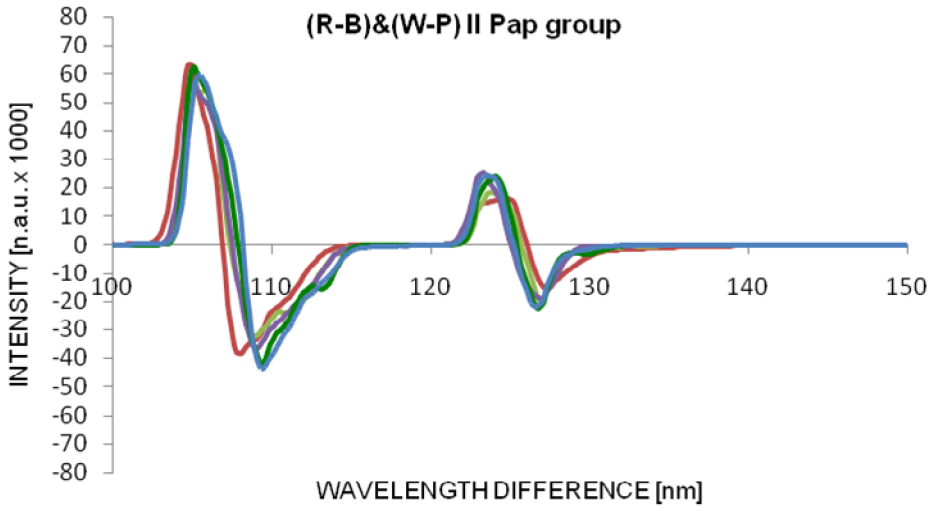

FIGURE 7.9
The OMIS spectra of cervical samples collected from 5 different patients diagnosed with Pap group II

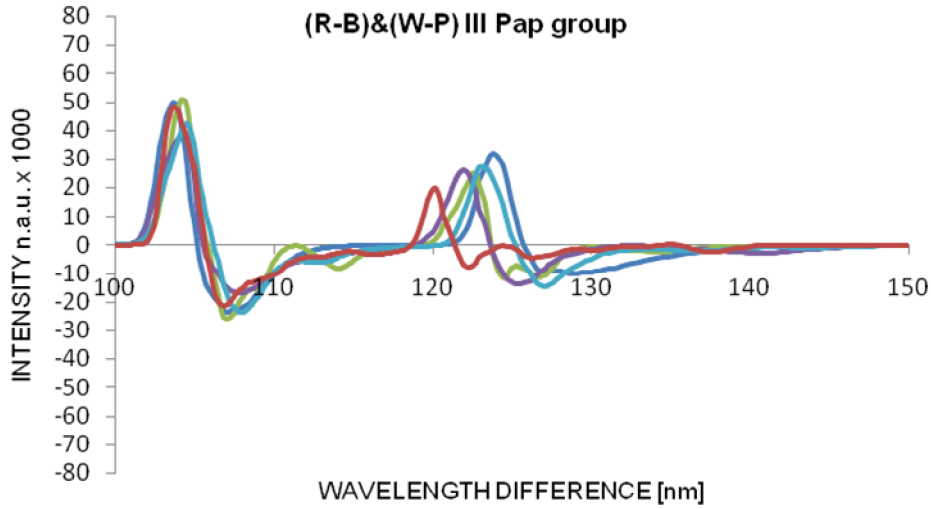

FIGURE 7.10
The OMIS spectra of cervical samples collected from 5 different patients diagnosed with Pap group III

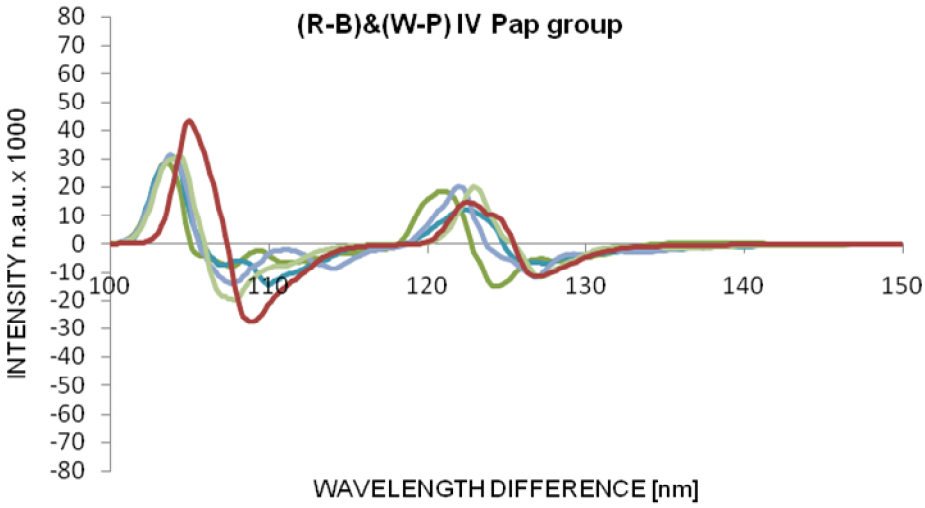

FIGURE 7.11
The OMIS spectra of cervical samples collected from 5 different patients diagnosed with Pap group IV

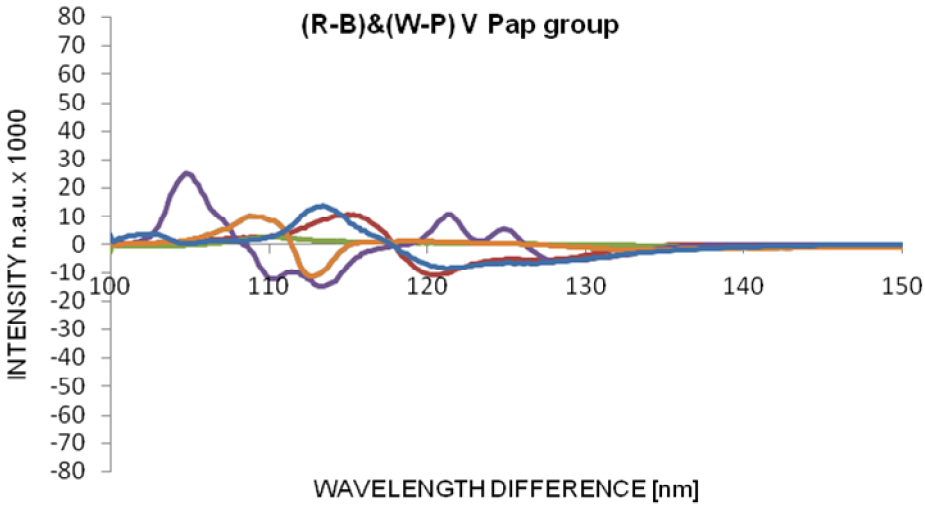

FIGURE 7.12
The OMIS spectra of cervical samples collected from 5 different patients diagnosed with Pap group V

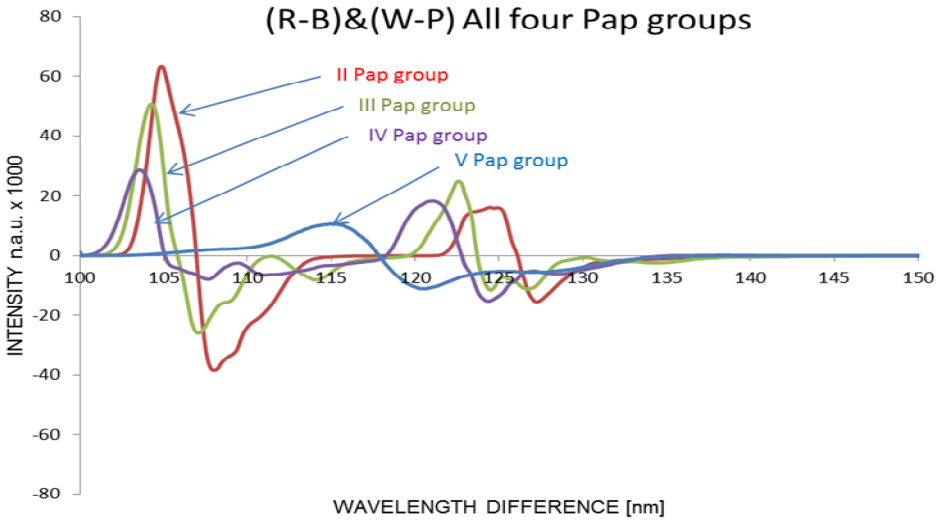

FIGURE 7.13
The OMIS spectra of cervical samples from all four Pap groups

The diagnosis of colon epithelial tissue using the Opto-magnetic imaging spectroscopy

The obtained data were processed and the results are presented with diagrams and tables with the characteristic values. By analyzing the intensities of the peaks that occur at specific wavelength difference, and the results obtained by histopathology analysis, it was observed that the OMS method shows sensitivity between healthy tissue and tumor tissue. Evidently, there are shift differences of wavelengths where the characteristic peaks occur. It is also apparent that there is a difference in the activity of tissues in the paramagnetic and diamagnetic zones.

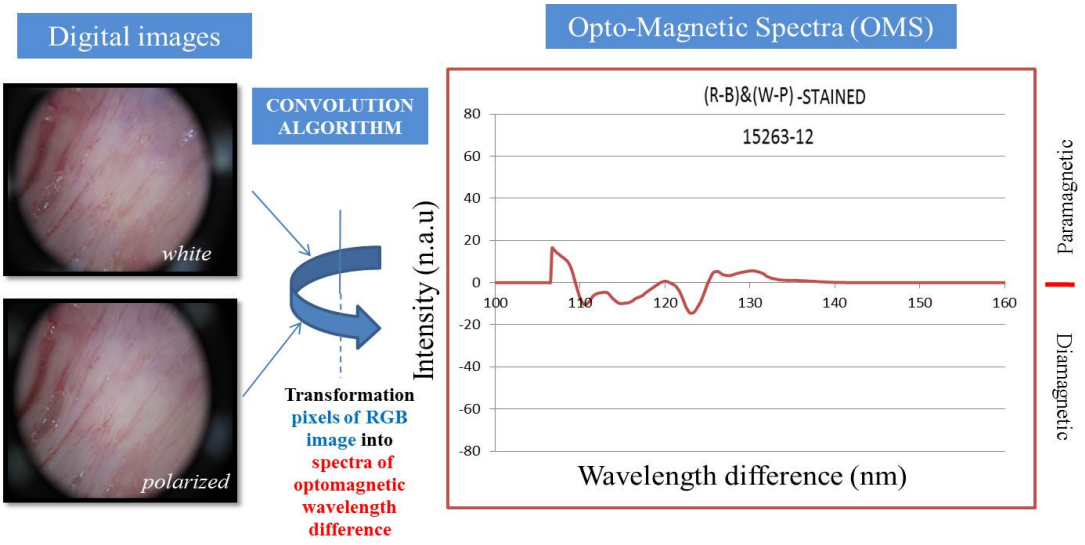

FIGURE 7.14
Image processing and the obtained characteristic diagram

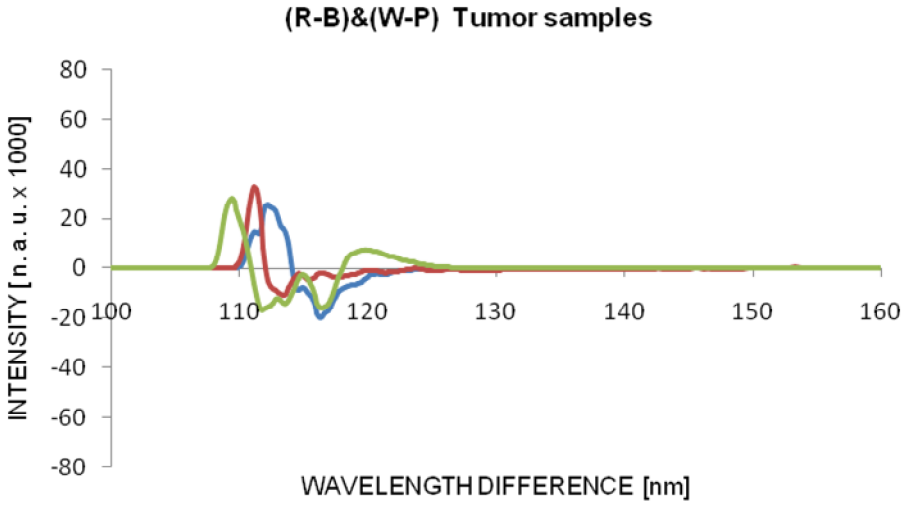

FIGURE 15
The diagram of the three examined colon tumour samples

TABLE 7.1
Characteristic peaks, wavelength differences at which they occur and the intensity of the three tumour samples

NUMBER OF TUMOR SAMPLES	I MAXIMUM		I MINIMUM	
	WD (nm)	I	WD (nm)	I
sample 1	25.356	112.083	-17.754	116.036
sample 2	32.808	111.117	-8.146	112.65
sample 3	27.574	109.196	-14.795	111.502

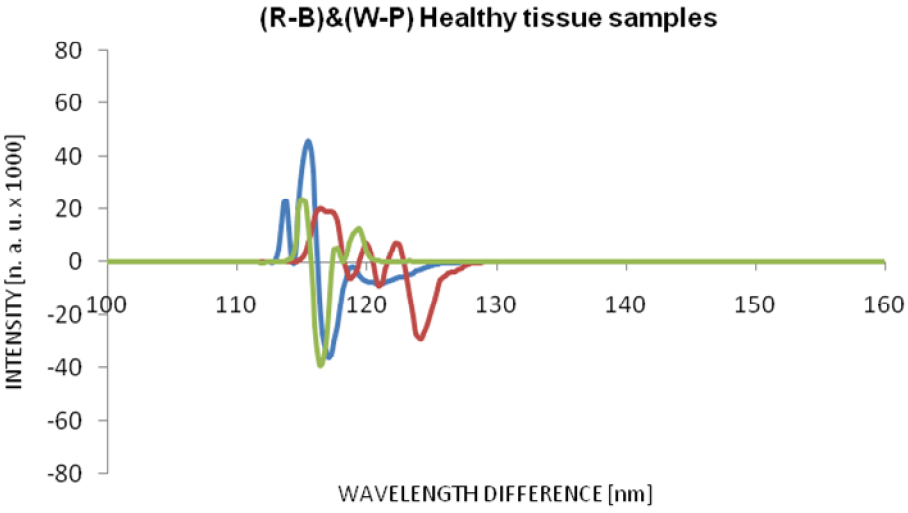

FIGURE 7.16
The diagram of the three examined healthy colon tissues

TABLE 7.2
Characteristic peaks, wavelength differences at which they occur and the intensity of the healthy tissue samples

NUMBER OF HEALTHY TISSUE SAMPLES	I MAXIMUM		I MINIMUM		II MAXIMUM		II MINIMUM	
	WD (nm)	I	WD (nm)	I	WD (nm)	I	WD (nm)	I
sample 1	22.417	113.614	-0.602	114.149	43.698	115.341	-33.36	116.87
sample 2	17.277	116.036	-3.309	118.455	119.136	5.103	-27.07	123.832
sample 3	22.871	115.341	-32.503	116.423	6.044	118.189	-4.957	119.48

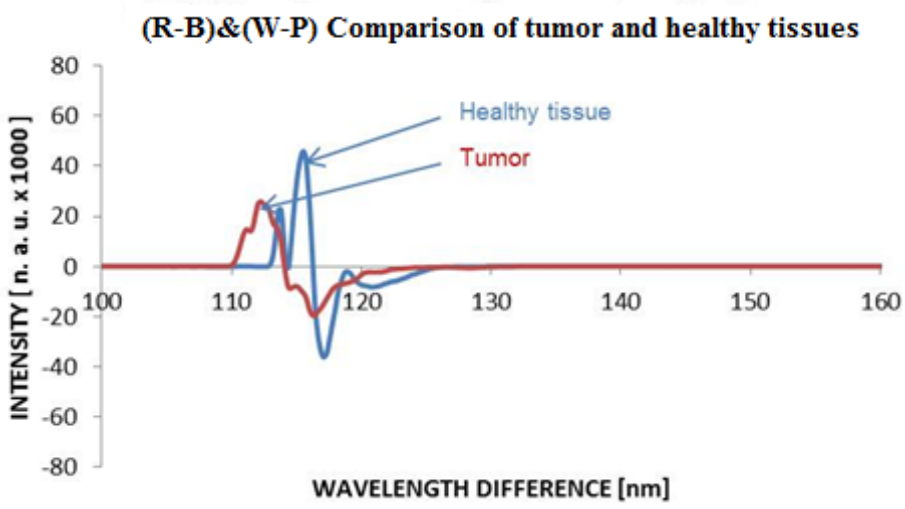

FIGURE 7.17
Differences between tumour and healthy colon tissues

The diagnosis of skin epithelial tissue using the Opto-magnetic imaging spectroscopy

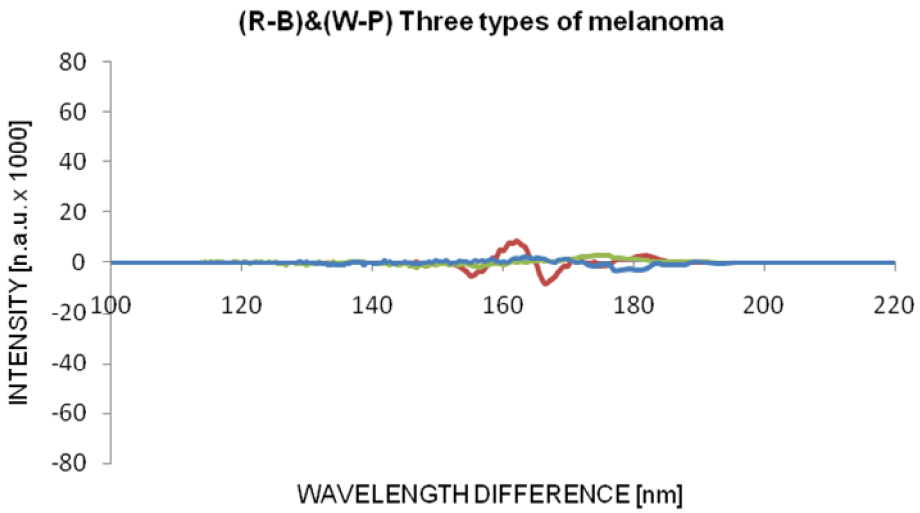

FIGURE 7.18
OMIS spectra for three melanoma en masse

By looking at the diagram above it can be seen that the intensity of the three melanomas is very small, practically unreadable and the wavelength difference vary from 120 up to 200 nm. The possible reason lies in the biophysical properties of the malignant cells and their activities.

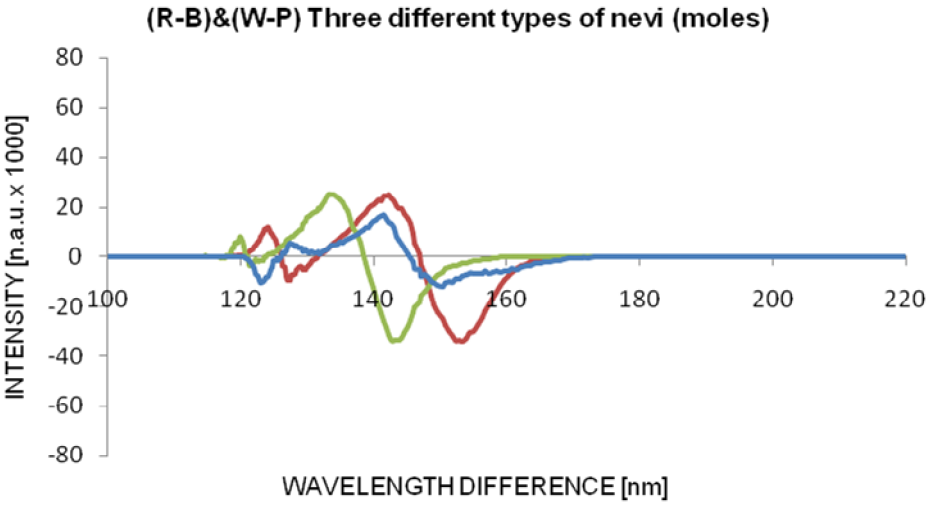

FIGURE 7.19
OMIS spectra for three nevi en masse

The comparison of these three nevi showed similarity in the shape of the curves (with some shifts), characteristic peaks and wavelength differences. There are two characteristic peaks on each diagram, one positive (132.263/20.706, 139.979/14.317, 140.372/21.827) and one negative (121.224/-1.491, 142.302/-31.299, 151.328/-29.893). Small variations exist probably because of the presence of many subtypes of nevi. One of the next steps in our study is to define the subgroups of nevi and melanoma using OMIS.

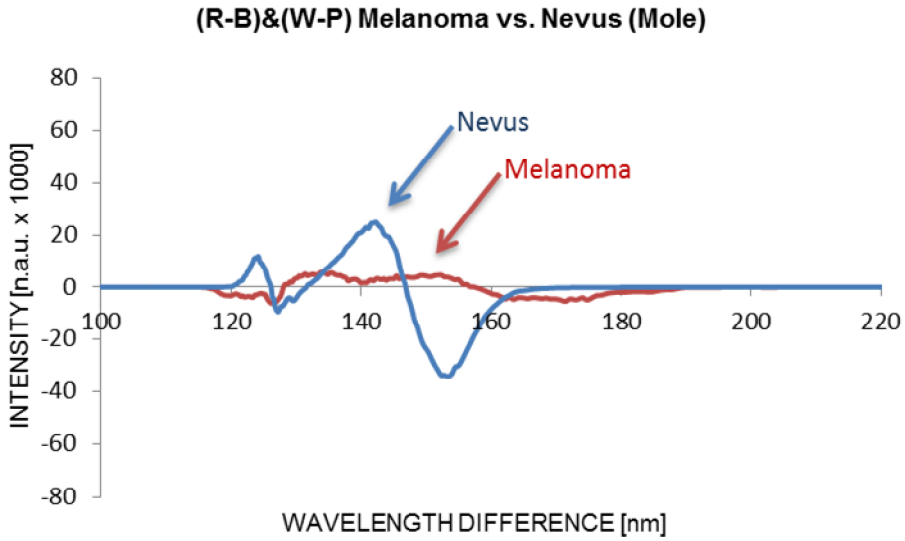

FIGURE 7.20
OMIS spectra for both melanoma and nevus (mole)

Statistical analysis

Summary statistics

Opto-magnetic imaging spectroscopy was developed with the purpose of serving as a non-invasive, economic, readily available, additional method for quick screening in outpatient conditions. It is based on tracking changes in paramagnetic/diamagnetic properties of tissues or cells which arise from the changes in the water matrix.
In the longitudinal study, the opto-magnetic spectra of tissues and cytological samples were collected over time for three types of healthy or benign changes of tissues and cells (healthy colon mucosae, nevus and cervical cytological samples of II Pap group) and malign changes (colon cancer, melanoma and cervical cytological samples of V Pap group). Cervical cytological samples were also collected for transition disease states: Pap group III and Pap group IV. However, in order to simplify the problem only two extreme groups – Pap II and Pap V were analysed because it was expected that the difference between them would be more evident and therefore easier to observe.
The types of tissues or cytological smears and the corresponding number of cases for which the opto-magnetic spectra were acquired, are presented in Table 7.3. The collected data comprise of a database of opto-magnetic spectra for healthy and cancerous changes in colon tissue, skin and cervical cells.

In order to estimate an overall tendency of changes in opto-magnetic spectra, a mean opto-magnetic spectrum for each study group (from Table 7.3) was calculated and presented in Figures 7.21-7.23.

TABLE 7.3
Types and sizes of study groups

Sample type	Number of cases	Sample type	Number of cases
Healthy colon mucous tissue	**55**	**Colon cancer tissue**	**57**
Naevus	**48**	**Melanoma**	**48**
Stained Pap smears on microscopic slides – II Pap group	**67**	**Stained Pap smears on microscopic slides – V Pap group**	**70**

The mean opto-magnetic spectra of malignant changes compared to the healthy state or benign changes in tissues and cells show decreased intensity values. This decrease is consistent in all cases of malignancy – in skin, colon and cervix cells.

A water molecule is composed of an oxygen atom with a paramagnetic value of 1.34×10^{-6} and two hydrogen atoms with a diamagnetic value of -2.48×10^{-8} for each of them. A single isolated water molecule is diamagnetic, with a mass magnetic susceptibility of -9.05×10^{-9}. Bulk water, in its pure form, makes dimer, trimmer and higher water clusters, showing both paramagnetic and diamagnetic properties (the average value of paramagnetism is 1.2 nT, and diamagnetism 2.3 nT), and in between the water constantly oscillates [44,45]. The opto-magnetic imaging spectrum based on an absorption difference (in order two, 100 times), of blue (B) and red ® channels of visible light may identified this dynamic.

In tumour cells and tissues, the state of water is altered [35-37, 46] and from the opto-magnetic spectra point of view for cancerous cells and tissues, it is evident that the paramagnetic/diamagnetic dynamics of water in diseased cells and tissues is disrupted compared to healthy tissue. This altered state of water is expressed through changes in the paramagnetic/diamagnetic properties of water and can thus be used as a classification criterion between healthy and cancerous states.

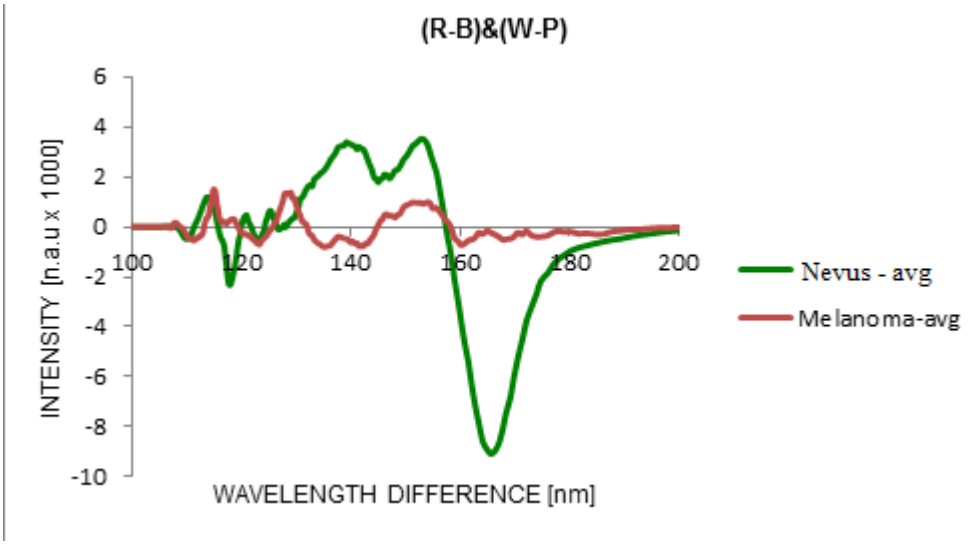

FIGURE 7.21
Comparison of the mean opto-magnetic spectra for the dataset of 48 melanoma cases and the mean opto-magnetic spectrum for the dataset of 48 nevus cases

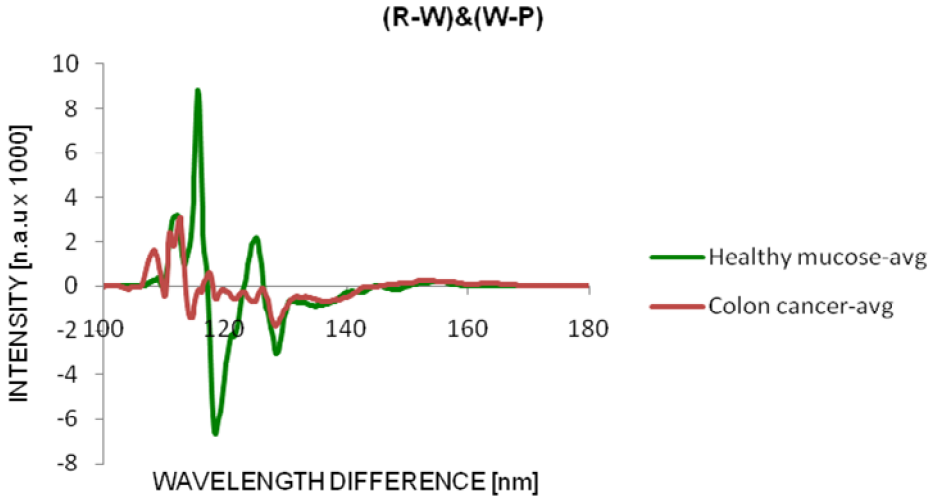

FIGURE 7.22
Comparison of the mean opto-magnetic spectrum for the dataset of 55 cases of healthy colon mucosa and the mean opto-magnetic spectrum for the dataset of 57 cases of colon cancer

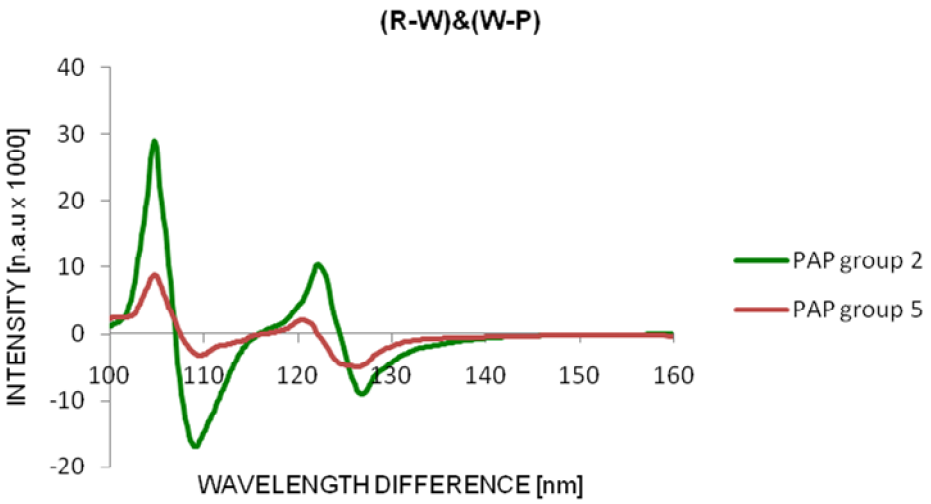

FIGURE 7.23
Comparison of the mean opto-magnetic spectrum for the dataset of 67 cases of II Pap group stained cervical smears and the mean opto-magnetic spectrum for the dataset of 70 cases of V Pap group stained cervical smears

The classification results

Generally, classification is a data mining function whose goal is to accurately predict class labels of instances whose attribute values are known, but class values are unknown. In this study the goal of the classifier is to correctly predict the class – healthy or cancer, based on the opto-magnetic spectra of tissue or cytology sample.

This study was concerned with the identification of three types of cancer: colon cancer, skin cancer (melanoma) and cervical cancer (PAP group V), therefore the classification was performed for three independent datasets of opto-magnetic spectra for cancer and healthy cases. For colon cancer and melanoma, opto-magnetic images were acquired from the tissue directly, while in the case of cervical cancer the images were acquired from stained cytological smears on microscopic slides. All these cases were assigned to a class of cancer cases. For the control group, the opto-magnetic images were taken of healthy colon mucosae, skin nevi (benign skin changes) and of stained cytological smears on microscopic slides (II Pap group). These cases were assigned to a class of healthy cases. The types of samples and the corresponding number of opto-magnetic spectra, used as input in the classification algorithms, are presented in Table 7.4. Two opto-magnetic spectra from the cervix database were detected as outliers and removed from further analysis.

TABLE 7.4
The types and sizes of three datasets of opto-magnetic spectra used for classification
For these three datasets, several classifying methods were applied (Soft Independent modelling of class analogies – SIMCA, k- nearest neighbours – kNN, support vector machine – SVM etc.) in order to distinguish differences between healthy and cancer cases, but so far, the most promising results were obtained using Naïve Bayes classification with kernel density estimation. All analysis of data was performed using statistical software R [46]

Material	Sample type	Total number of cases	Number of cancer cases	Number of healthy cases
Colon	**Tissue**	**112**	**55**	**57**
Skin	**Tissue**	**96**	**48**	**48**
Cervix	**Stained cytological smear**	**135**	**66**	**69**

A naïve Bayes (NB) classifier is an important classifier for data mining and applied in many real world classification problems because of its high classification performance. It is a simple probabilistic classifier based on: (a) Bayes theorem, (b) strong (naive) independence assumptions, and (c) independent feature models [48]. Naïve Bayes classification with kernel density estimation, or so called "flexible Bayes" is an extension of the naïve Bayes classifier which uses a kernel density estimation where the density of each continuous variable is estimated averaging over a large set of kernels. The method performs well in domains that violate the normality assumption and, in general, this flexible Bayesian classifier generalises better than the version that assumes a single Gaussian [49].

In this study, to estimate the performance of the classifier, a 10-fold cross-validation approach was used. In the 10-fold cross-validation, the entire dataset is divided into 10 mutually exclusive subsets. Each fold is used once to test the performance of the classifier that is generated from the combined data of the remaining nine folds, leading to 10 independent performance estimates and thus ensuring optimal utilization of the available data. Given the relatively small size of available samples, this choice seemed to be the best solution.

Evaluation of the classifier performance was done using three performance measures: specificity, sensitivity and accuracy:

$$\text{Specificity: } \frac{\text{TN}}{\text{TN+FP}} \tag{1}$$

$$\text{Sensitivity: } \frac{\text{TP}}{\text{TP+FN}} \tag{2}$$

$$\text{Accuracy: } \frac{\text{TP+TN}}{\text{TP+TN+FP+FN}} \tag{3}$$

where TP, TN, FP and FN denote numbers of true positives, true negatives, false positives and false negatives, respectively.

A true positive (TP) is the number of cases correctly identified as cancer, while a true negative (TN) is the number of cases correctly identified as healthy. A false negative (FN) is the number of cancer cases

incorrectly identified as healthy, and a false positive (FP) is the number of healthy cases incorrectly identified as cancer.

As an additional measure of classifier accuracy, Cohen's kappa [50] was calculated. Cohen's kappa measures classifier accuracy, while compensating for successes due to chance. Cohen's Kappa is defined as:

$$\mathrm{K} = \frac{\mathrm{p_0} - \mathrm{p_c}}{1 - \mathrm{p_c}}, \tag{4}$$

where p_0 is the total agreement probability, and p_c is the ''agreement'' probability which is due to chance. It is more convenient to calculate Kappa using counts from the confusion matrix, rather than probabilities:

$$K = \frac{N \times \sum_{i=1}^{I} x_{ii} - \sum_{i=1}^{I} x_{i.} x_{.i}}{N^2 - \sum_{i=1}^{I} x_{i.} x_{.i}}, \tag{5}$$

where x_{ii} is the count of cases in the main diagonal, N is the number of examples, and x_i, x_i are the columns and rows total counts, respectively. Cohen's kappa statistics range from -1 (total disagreement) through 0 (random classification) to 1 (total agreement) [51].

Table 7.5 gives a summary of the classification results for the three datasets of inputs – colon samples, skin samples and cervix smears samples. Detailed prediction results are presented in the form of confusion matrices (Tables 7.6-7.8).

TABLE 7.5
Summary of classification results using Naïve Bayes classifier with kernel density estimation

Performance measures	Specificity [%]	Sensitivity [%]	Accuracy [%]	Kappa
Skin	**87.04**	**97.62**	**91.67**	**0.833**
Colon	**100**	**92.98**	**96.43**	**0.9286**
Cervix	**78.16**	**97.92**	**85.18**	**0.7018**

TABLE 7.6
Confusion matrix for Cervix dataset

Confusion matrix		Predicted	
		Healthy	**Cancer**
Actual	**Healthy**	**68**	**19**
	Cancer	**1**	**47**

TABLE 7.7
Confusion matrix for Skin dataset

Confusion matrix		Predicted	
		Healthy	Cancer
Actual	Healthy	41	1
	Cancer	7	47

TABLE 7.8
Confusion matrix for Colon dataset

Confusion matrix		Predicted class	
		Cancer	Healthy
Actual	Cancer	53	0
	Healthy	4	55

As it is shown in the results above, the chosen data mining method provide models that possess a high degree of accuracy. Minimal accuracy was achieved for the cytological samples of cervical cells, but 85.18% of accurately predicted cases is still a very high number. The best results were achieved for the classification between healthy and cancerous colon tissue, where the accuracy was 96.46%. It should be noted that the opto-magnetic spectra developed for the images of cytological samples are quite complex compared to the images of colon tissue, where even untrained personnel can easily distinguish between an image of colon cancer and colon mucosae, while in the case of cytological samples it is rather difficult. The achieved accuracy results are therefore very logical given the fact that the task for the classifier is the simplest in the case of colon tissue, more complex in the case of skin changes, and very complex for cytological samples.
Kappa statistics for all three datasets is high, close to 1, which excludes the possibility that this classification result is due to chance. The results of prediction based on the opto-magnetic spectra confirm the potential of the Opto-magnetic imaging spectroscopy method to discriminate between healthy and cancer cases.
However, even though these results are promising, it should be noted that the size of the datasets is still limited for final conclusions. It is also possible that other data mining methods could be more successful in discriminating between the opto-magnetic spectra of healthy and cancer cases.

Conclusion

Opto-magnetic Imaging Spectroscopy was applied *in vitro* and *in vivo* on cervical, colon, and skin samples. Research included 280 cervical samples, 112 colon samples and 96 skin samples. The opto-magnetic spectra showed a good differentiation between healthy and cancerous samples based on characteristic OMIS spectra intensities and peak positions. It is shown that spectra intensity decreases

towards lower values in cases of precancerous and cancerous tissues in all three kinds of epithelial tissue. Classification results proved a high degree of accuracy in cancer detection (skin 91.67%, colon 96.43%, cervix 85.18) using the OMIS method. Research efforts are underway and are geared towards expanding the databases of the opto-magnetic spectra of cancer and healthy cases, and also research of an optimal classification method in order to develop a method which would complement the efforts of medical professionals in quick screening and early cancer diagnostics.

Acknowledgment

This research has been funded by the Ministry of Education, Science and Technological Development of the Republic of Serbia, through Project III 41006: *Development of methods and techniques for early diagnostic of cervical, colon, oral cavity cancer and melanoma based on a digital image and excitation-emission spectrum in visible and infrared domain*. Also, this research is partially funded by Tempus project: „Studies in Bioengineering and Medical Informatics - BIOEMIS“, 530423-TEMPUS-1-2012-1-UK-TEMPUS-JPCR. We are particularly grateful to Zoran Krivokapić (School of Medicine, Clinical Centre of Serbia, University of Belgrade), Jadran Bandić (ORS Hospital, Belgrade) and Milena Papić-Obradović (Clinic for Gynecology and Obstetrics “Narodni Front”, Belgrade) who provided samples, and therefore made it possible for us to realise this research. Also, we are thankful to the staff at each clinic who helped and supported this research. In the initial stage of research MySkin,Inc, USA partially supported this investigation.

References

1. Longo LD. Harrisons Hematology and Oncology. United States: Mc Graw-Hill Companies, Inc.; 2010.
2. International Agency for Research on Cancer, 2010: Cancer Incidence and Mortality Worldwide GLOBOCAN 2008, IARC CancerBase No. 10 Lyon, France: http://globocan.iarc.fr. (accessed May 2011).
3. Rogers HW, Weinstock MA, Harris AR, et al. Incidence estimate of nonmelanoma skin cancer in the United States 2006. Archives of Dermatology 2010; 146(3) 283-287.
4. American Cancer Society. Cancer Facts & Figures 2013. http://www.cancer.org (accessed 31 January, 2013).
5. Cancer research UK: the UK leading cancer charity: Cancer research UK. http://www.cancerresearchuk.org (accessed 11 May, 2012).
6. Kuehnel W. Color Atlas of Cytology, Histology and Microscopic Anatomy. Thieme; 2003.
7. Berman I. Color Atlas of Basic Histology. LANGE Basic Science; 2003.
8. Marieb EM. Human Anatomy and Physiology. Benjamin/Cummings; 1995.
9. Lommel V., Alfons TL. From cells to organs: a histology textbook and atlas. Springer; 2002.
10. Pratt R. Epithelial Cells, AnatomyOne. Amirsys, Inc. Retrieved; 2012.
11. Breitkreutz D., Mirancea N., Nischt R. Basement membranes in skin: Unique matrix structures with diverse functions? Histochemistry and cell biology 2009; 132(1) 1–10.
12. McGrath JA., Eady RA., Pope FM. Rook's Textbook of Dermatology. Blackwell Publishing; 2009.
13. Thomas P., Habif MD. Clinical Dermatology: Expert Consult - Online and Print. Elsevier; 2009.
14. McCracken T. New Atlas of Human Anatomy, China: Metro Books, 2000.

15. Madison KC. Barrier function of the skin: "la raison d'être" of the epidermis. J Invest Dermatol 2003; 121(2) 231-41.
16. Proksch E, Brandner, JM., Jensen JM. The skin: an indispensable barrier, Exp Dermatol 2008; 17(12) 1063–72.
17. Marks JG., Miller JJ. Lookingbill and Marks' Principles of Dermatology: Expert Consult Online and Print. Saunders, 2013.
18. Hoffman B., Schorge J., Schaffer J., Halvorson L., Bradshaw K., Cunningham G, Williams Gynecology. The McGraw-Hill Companies, 2012.
19. Cunningham F., Leveno K., Bloom B., Hauth J., Rouse D., Spong C. Williams Obstetrics.The McGraw-Hill Companies, 2009.
20. Ross MH. Hystology A Text and Atlas. Philadelphia, PA: Lippincott Williams & Wilkins; 2010.
21. Gordon P., H., Santhat N. Neoplasms of the colon, rectum, and anus. New York: Informa, Healthcare; 2007.
22. Chang J., Huang Y., Wu P., Chen C., Huang S., Tsai Y. Characterization of human cervical precancerous tissue through the Fourier transform infrared microscopy with mapping method. Gynecologic Oncology 2003; 91(3) 577–583.
23. Sahu R., Mordechai S. Fourier transform infrared spectroscopy in cancer detection. Future Oncol. 2005; 1(5), 635–647.
24. Krishna C., M. et al., Raman spectroscopy studies for diagnosis of cancers in human uterine cervix. Vibrational Spectroscopy 2006; 41(1) 136–141.
25. Bellisola G., Sorio C. Infrared spectroscopy and microscopy in cancer research and diagnosis, Am J Cancer Res 2012; 2(1) 1-21.
26. Beljebbar A., Bouche O., Diebold M., D., Guillou P. J., Palot J., P., Eudes D., Manfait M. Identification of Raman spetroscopic markers for the characterization of normal and adenocarcinomatous tissues. Critical Reviews in Oncology/Hematology 2009; 72(3) 255-264.
27. Hammody Z., Argov S., Sahu R.K., Cagnano R.K., Moreha R., Mordechai S. Distinction of malignant melanoma and epidermis using IR micro-spectroscopy and statistical methods. Analyst 2008,133 372-378.
28. Koruga Dj., Tomic A. Method and algorithm for analysis of light-matter interaction based on spectral convolution. US Pat. App. No.61/061,852, 2008, PCT/US2009/030347, Publication No: WO/2009/089292, Publication Date: 2009-07-16.
29. Stamenković S., Kojić D., Matija L., Miljković Z., Babić B. Physical Properties of Contact Lenses Characterized by Scanning Probe Microscopy and OptoMagnetic Fingerprint. International Journal of Modern Physics B: Condensed Matter Physics; Statistical Physics; Applied Physics 2010; 24(6-7) 825-834.
30. Papić-Obradović M., Kojić D., Matija L. Opto-Magnetic Method for Epstein – Barr Virus and Cytomegalovirus Detection in Blood Plasma Samples. Acta Physica Polonica A 2010; 117(5) 782-784.
31. Koruga Dj., Miljković S., Ribar S., Matija L., Kojic D. Water Hydrogen Bonds Study by Opto-Magnetic Fingerprint. Acta Physica Polonica A 2010; 17(5) 777-781.
32. Koruga Dj., Bandić J., Janjić G., Lalović C., Munćan J., Dobrosavljević Vukojević D. Epidermal layers characterisation by opto-magnetic spectroscopy based on digital image of skin. Acta Physica Polonica A 2012; 121(3) 1111-1115.
33. Matija L., Koruga Dj. Value of action as a criteria for classical and quantum object consideration on molecular level. In: Šumarac D, Kuzmanović D. (eds.): proceedings of the First International Congress of Serbian Society of Mechanics, 10-13 April 2007, Kopaonik, Serbia.

34. Lide D.R., editor. Handbook of Chemistry and Physics, 77th Edition. Boca Raton: CRC Press; 1996.
35. Duck,.A.F., Physical properties of tissues: A Comprehensive reference book, Academic Press, London, 1990.
36. Chaplin M. Do we underestimate the importance of water in cell biology? Nature Reviews Molecular Cell Biology 2006; 7(11) 861-866.
37. McIntyre, G.I. Increased cell hydration promotes both tumor growth and metastasis: A biochemical mechanism consistent with genetic signatures. Medical Hypothesis 2007; 69 1127-1130.
38. Denny L. Cytological Screening for Cervical Cancer Prevention. Best Practice & Research Clinical Obstetrics and Gynaecology 2012; 26 189-196
39. Rosa M., Pragasam P., Saremian J., Aoalin A., Graf W., Mohammadi A. The Unsatisfactory ThinPrep Pap Test: Analysis of Technical Aspects, Most Common Causes, and Recommendations for Improvement. Diagnostic Cytopathology 2013;41(7) 588-94.
40. Walsh MJ. et al. ATR microspectroscopy with multivariate analysis segregates grades of exfoliative cervical cytology. Biochemical and Biophysical Research Communications 2007; 352 213-219
41. Pijanka J.K et al. FTIR microspectroscopy of stained cells and tissues. Application in cancer diagnosis. Spectroscopy 2010; 24(1-2) 73-78
42. Jeftić B. Early diagnosis of cervical cancer diagnosis using Optomagnetic spectroscopy. In Papić-Obradović M. (ed.) Early diagnosis of epithelial tissue cancer. Belgrade: Don Vas; 2012. p311-324 (in Serbian).
43. Papić-Obradović M., Jeftić B., Koruga Đ. Optospectroscopy and opto-magnetic spectroscopy in early detection of cervical cancer. In: proceedings of the National Symposium of the 57. Ginekološko-akušerska nedelja, 6-7 June 2013, Belgrade, Serbia. (in Serbian).
44. Koruga Dj., Golden mean harmonized water and aqueous solutions, International Publication Patent Number WO 2008/097922 A2, Publication Date 14.August 2008.
45. Koruga Dj., Paramagnetic/diamagnetic properties of water and Aqueous solutions: classical/quantum approach for Biomedical applications. In: Book of Abstracts, International conference on Water, Hydrogen Bonding Nanomaterials and Nanomedicine, 2010, Banja Luka, Republic of Srpska, Bosnia and Herzegovina. Banja Luka: Academy of Science and Arts of the Republic of Srpska; 2010.
46. McIntyre G.I. Cell hydration as the primary factor in carcinogenesis: A unifying concept. Medical Hypotheses 2006; 66 518-526.
47. R Development Core Team, 2007. R: A language and environment for statistical computing. R Foundation for Statistical Computing, Vienna, Austria. ISBN 3-900051-07-0. http://www.R-project.org
48. Farid D., Zhang L., Rahman C., Mofizur H., Strachan, R., Hybrid decision tree and naïve Bayes classifiers for multi-class classification tasks, Expert Systems with Applications, 2013, http://dx.doi.org/10.1016/j.eswa.2013.08.089
49. Soria D., Garibaldi J.M., Ambrogi F., Biganzoli E.M., Ellis I.O. A 'non-paramteric' version of the naïve Bayes classifier. Knowledge-Based Systems 2011; 24 775-784.
50. Cohen J.A. Coefficient of agreement for nominal scales. Educational and Psychological Measurement 1960; 20 37–46.
51. Ben-David A. Comparison of classification accuracy using Cohen's Weighted Kappa. Expert Systems with Applications 2008; 34 825-832.